Investigation of Electric Field Enhancement and Effects of Discharge Severity in an Insulated Power Cable with Multiple Gaseous Cavities

U. Musa [1*], A. A. Mati [1,2], A. A. Mas'ud [3], G. S. Shehu [1], S. H. Sulaiman[1], J. M. Rodriguez-Serna [4]

[1]Department of Electrical Engineering, Ahmadu Bello University, Samaru, Zaria, Nigeria
[2]Centre for Energy Research and Training (CERT), Ahmadu Bello University, Samaru, Zaria, Nigeria
[3]Department of Electrical Engineering, Jubail Industrial College, Jubail, KSA
[4]Departamento de Ingeniería Eléctrica, Facultad de Ingeniería, Universidad de Antioquia (UdeA), Medellín, Columbia.

ABSTRACT: Gaseous cavities in the insulation of high voltage (HV) cables affect the electric field distribution and increase the electrical stress. This accelerates material ageing and creates partial discharge (PD) regions, which can cause cable failure. In this study, a simulation approach using a Finite Element Method (FEM) has been deployed to evaluate the discharge activity and electric field variation in cross-linked polyethylene (XLPE) insulated power cables. 2-Dimension models corresponding to sections of a practical three-core XLPE insulated cable were developed using COMSOL Multiphysics. Multiple cavities of different dimensions and configurations were considered. The results show that the electric field varies depending on the configuration and dimensions of the cavity. It was found that maximum field strength magnitude depends on the cavities, arrangement and location; an increase of up to 68.7% when compared to the case without cavities.

KEYWORDS: Cross-linked polyethylene (XPLE), electric field strength, cavity, high voltage, COMSOL Multiphysics

[Received Nov. 4, 2022; Revised June 18, 2023; Accepted July 29, 2023] Print ISSN: 0189-9546 | Online ISSN: 2437-2110

I. INTRODUCTION

In power systems, high voltage (HV) installations are crucial since their failure may result in partial or whole system outages (Mas'ud *et al.*, 2016; Mas'ud *et al*., 2017; Gouda, *et al*., 2018). Power cables, which are typically used at all levels of the power network, are among the most important of these devices. According to recent studies, electric power cables used for HV and medium voltage (MV) applications constitute close to 15 – 20 % of the overall power distribution network (Gouda, *et al*., 2018, Do Nascimento *et al*., 2019). As a result, utilities must maintain adequate maintenance of these assets for the bulk power system to operate efficiently and reliably. Electric power cables, like other HV switchgear, are often exposed to persistent operating stress that might be damaging to the equipment (Subramaniam, *et al*., 2021, Feng *et al*., 2021). The kind and nature of insulation systems are essential to the continued existence of service equipment (Kuffel, *et al*., 2000). For many years, cross-linked polyethylene (XLPE) insulated power cables have been utilized in high- and medium-voltage (MV) applications (Sharshir, *et al.*, 2022). XLPE has outstanding dielectric, thermal, and mechanical qualities, allowing it to endure forces other than the primary electrical stress (Afia, *et al*., 2021; Pandey and Singh, 2021).

The presence of defects in the insulation systems of power cables poses a serious threat to the lifespan of the equipment (Choudhary, *et al.*, 2022). They operate as areas of increased field activity, which leads to partial discharge (PD) activities, causing electrical ageing and ultimately failure (Rodríguez-Serna, *et al*., 2020; Pan, *et al*., 2019). Research involving PD activity in power cables has been thoroughly investigated for diagnostic purposes (Refaat, *et al*., 2018; Zhang, *et al*., 2021). Specifically, (Zhang, *et al*., 2021) reviewed the PD mechanism and models utilized in the power cable PD study. PD models were thoroughly investigated, ranging from a capacitor model to an analytical model, and then the finite element analysis (FEA) based model, each having advantages and disadvantages. Depending on the objectives of the research, a specific model might be used. Two methods are being used for PD detection in cables i.e. online and offline. Off-line testing often employs alternating current voltage with resonant test equipment, damped alternating current, and extremely low frequencies down to 0.01 Hz. Online platforms are now becoming more prevalent. Sensors used for PD measurements in cables are mostly inductive and capacitive. The authors suggested that the correlation between discharge activity testing on laboratory samples and PD assessments in the field should be improved. Denoising must be enhanced on both the algorithm and the sensor levels. Precise PD diagnosis remains difficult because the relationship between PD and ageing is still not well understood.

Furthermore, the modelling of a discharging cavity's field distribution is extensively established in the literature (Joseph, *et al*., 2019; Rodríguez-Serna and Albarracín-Sánchez, 2019; Ragusa, *et al*., 2020; Morsalin, *et al*., 2020; Morsalin and Phung, 2020; Musa, *et al*., 2021). Most of the aforementioned studies considered a single cavity in cables or solid insulation, without taking into consideration the electric potential or field

*Corresponding author: umusa@abu.edu.ng

doi: http://dx.doi.org/10.4314/njtd.v18i4.1435

variation of different geometries or the position of the cavity in the insulation. Generally, research involving multiple cavities is limited, particularly for different cavity shapes and positions. One technique to contribute to the understanding of the PD phenomenon is to determine the electric field distribution throughout the cable insulation in the presence of multiple cavity defects. A physical model of the cable with the occurring cavities within the insulation must be generated in this respect, to analyse the field strength for PD prognosis before total failure.

Previous studies have focused on analysis in cables with single cavity defects, however multiple cavities can appear where PDs can appear simultaneously, and also synergetic phenomena can appear resulting in an acceleration of the PD induced degradation process. This study also presents the expected magnitudes of PD discharges in defects inside cables of practical dimensions.

II. THEORETICAL CONCEPT

A. The Geometry of the Case Study Model

The structural features of an insulated power cable are derived from the literature (Meziani, *et al*., 2016). As shown in Figure 1, a physical model in 2D geometry was developed to reflect the multiple cavities inside a segment of the cable. It consists of 6 sub-domains depicting the XLPE insulation and its screen, the cable's conductor and its screen, followed by the metallic sheath. There are also three gaseous cavities, each 1mm in diameter arranged vertically, horizontally, and in a random configuration at various locations (Table 1). The material characteristics that make up the various components of the power cable are the same as those utilized in the (Meziani, *et al*., 2016) and are shown in Table 2.

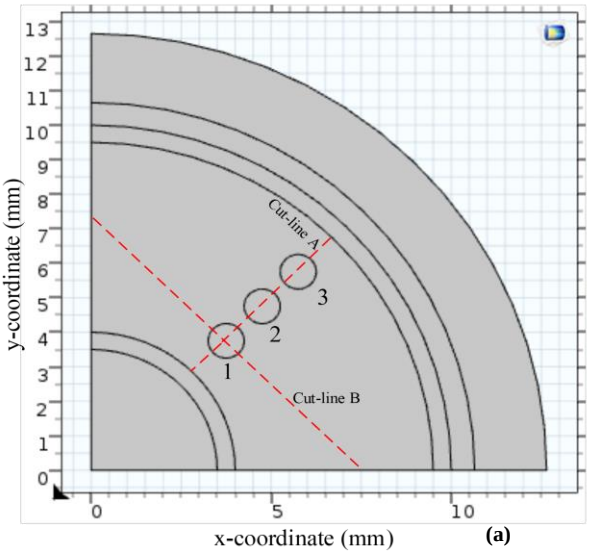

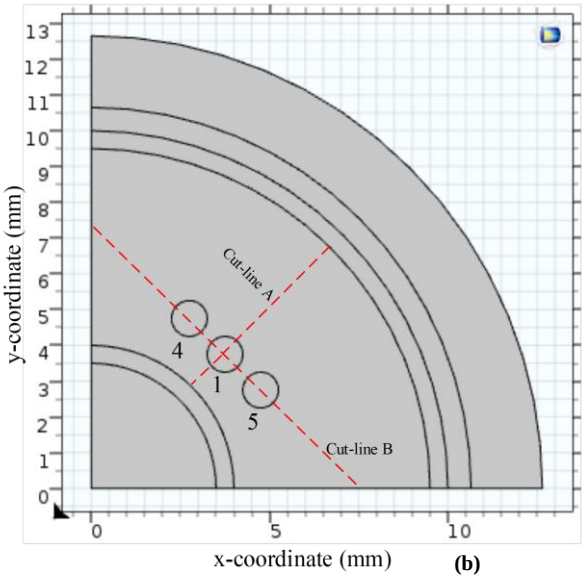

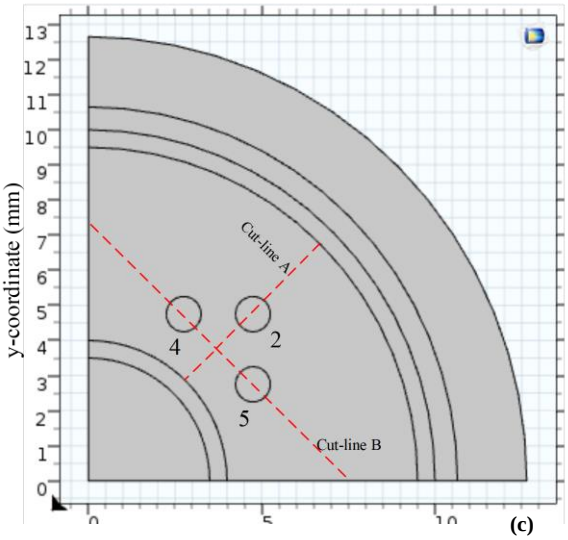

Fig. 1. The cable section's 2D geometry including the three gaseous cavities arranged (a) vertically (b) horizontally and (c) arbitrarily.

Table 1: Location of the cavities

Location of the cavity	x-axis position (mm)	y-axis position (mm)
1	3.388	4.102
2	4.388	5.102
3	5.388	6.102
4	3.402	4.135
5	3.380	4.08

Table 2: The power cable parameters

Parameters	Values
Cavity volume density	1.205 kg/m^3
Outer sheath electrical conductivity	1×10^{-10} S/m
Conductor electrical conductivity	3.03×10^{7} S/m
Metallic sheath electrical conductivity	5.99×10^{7} S/m
Cavity's initial electrical conductivity	1×10^{-100} S/m
Insulation material's relative permittivity	2.3
Cavity's relative permittivity	1
Insulation material volume density	561 kg/m^3
Insulation material electrical conductivity	1×10^{-15} S/m
Cavity final electrical conductivity	5×10^{-4} S/m
Outer sheath relative permittivity	2.3
Semiconductor screen relative permittivity	500

B. Electric Field Estimation and the PD Model

In the model, the electric field is determined using the Maxwell's equations in partial differential form as are described below (Alsharif, *et al*., 2012).

$$\varepsilon_0 \varepsilon_r \vec{\nabla} \bullet \vec{E} = \varepsilon_0 \varepsilon \vec{\nabla} \bullet \left(-\vec{\nabla} V \right) = 0 \tag{1}$$

$$\vec{\nabla} \bullet \left(\sigma \vec{\nabla} V + \varepsilon_0 \varepsilon_r \vec{\nabla} \frac{\partial V}{\partial t} \right) = 0 \tag{2}$$

$$V = V_P * sin 2\pi ft \tag{3}$$

where V is the scalar potential at a general location, ε_r denotes the relative permittivity of insulation, ε_o denotes the relative permittivity of free space and σ is the material's electrical conductivity. For the statement of Eqns. (1)-(3), it is assumed there is not free charges and currents in the dielectric bulk, so there are not sources of magnetic fields, the media are linear, homogeneous and isotropic.

Understanding the discharge mechanism is crucial for modelling the PD event. Two things must happen before PD can happen (Gutfieisch and Niemeyer, 1995). First, there must be enough high electric stress in the cavity to cause a breakdown. This means that the voltage in the cavity must be greater than or equal to the PD inception voltage. Second, there needs to be an initial electron in the cavity to kick off the ionization process. The PD inception voltage can be calculated as a function of the inception field (E_{ip}), which is the average cavity field, using the following equation:

$$E_{ip} = \left(\frac{E}{g_p} \right) g_p \left\{ 1 + \frac{B}{\left(2 g_p r_c \right)^m} \right\}, \tag{4}$$

where m, B and (E/g_p) represent the gas ionization parameters, r_c is the radius of the cavity and g_p denotes the gas pressure within the cavity surface (Zhang, *et al*., 2021; Joseph, *et al*., 2019).

In this instance, a change in the cavity gas's conductivity state is used to represent the PD transient. In this case, the initial PD event is simulated by increasing the conductivity of the cavity's gas from a starting value (about zero) before the PD event to a higher value after the PD event. An increase in the cavity's conductivity (from a non-conducting to a conducting state) results in a decrease in the cavity's electric field strength. Throughout the PD event, the cavity's conducting state is maintained until the electric field strength magnitude drops below that of the extinction electric field strength magnitude. The value of σ_{cavm} was determined using the cavity's size and shape as follows (Zhang, *et al*., 2021; Joseph, *et al*., 2019):

$$\sigma_{cavm} = \frac{\beta e^2 M_e \gamma_e}{n_e c_e}, \tag{5}$$

where e stands for the electric charge of the electron, γ_e denotes the mean free path of the electron, c_e denotes the electrons's thermal speed, n_e denotes the electron mass, and *Me* denotes the density of the electron. Together, these components are written as:

$$M_{cavm} = \frac{q_m}{\pi (1.33) e r_c^3} \tag{6}$$

where q_m is the maximum physical charge magnitude obtained from measurement. In this study, all the PD parameters were drawn from the literature (Zhang, *et al*., 2021).

III. METHODOLOGY

Figure 2 shows a flowchart representation of the field simulation model. The created 2D model is implemented in COMSOL multiphysics utilizing the finite element analysis (FEA) approach by solving the electric currents equation in the software's AC/DC application module. The simulation time, which is determined by the number of time steps and mesh size, is optimized. To reach a reasonable computation time in the model, a 'Finer' mesh size with a 'Free Triangular' element is utilized. The meshes around the area of the geometry are refined, because of the requirement for a higher degree of accuracy in the electric potential calculations. After all sub-domains and boundaries have been appropriately established, the meshed model is subjected to a 'Duration Dependent' study with a simulation period of 5 x10^{-3} s. The time step is set to 2.5 x10^{-3} s. In COMSOL Multiphysics, the simulation start time, time step, and stop time are all set to 0:0.0025:0.005s. The occurrence of a PD in the multiple gaseous cavities is represented in COMSOL by evenly increasing the conductivities of the cavities (Gutfieisch and Niemeyer, 1995). Electric field magnitudes from the FEA-based model are measured and analysed before and after the PD event. It should be mentioned that the model was subjected to a 50Hz, 11 kV AC voltage throughout the simulation phase. These values correspond to real-world power lines encountered at distribution levels for subterranean applications.

IV. RESULTS AND DISCUSSION

A. Distribution of Electric field magnitudes for the three configurations (before and after the PD events)

Figure 3 depicts a surface plot of the simulation model's electric field distributions before and immediately after the first PD event. Figure 3a shows the gaseous cavities arranged vertically. It can be shown that the field intensity at the lower cavity (i.e the one close to the conductor) is higher than that at the middle and the upper cavity (Figure 3a). Because of the cavity's proximity to the source field, this kind of field strength

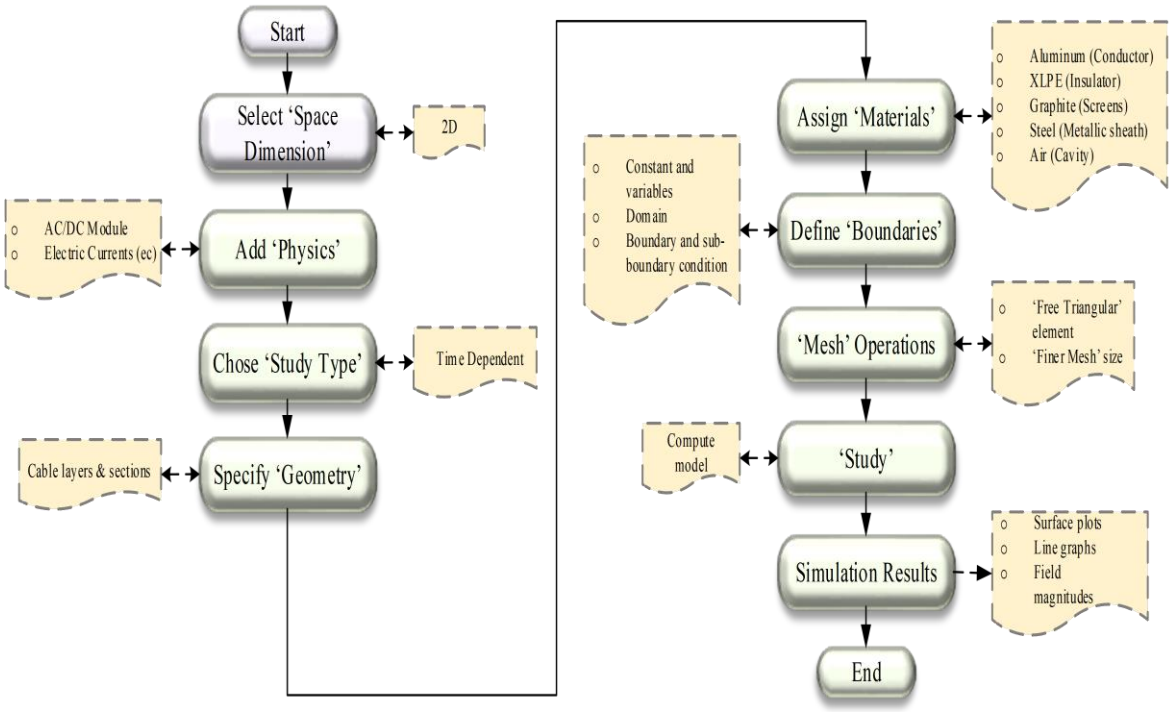

Figure 2. Field simulation model flowchart

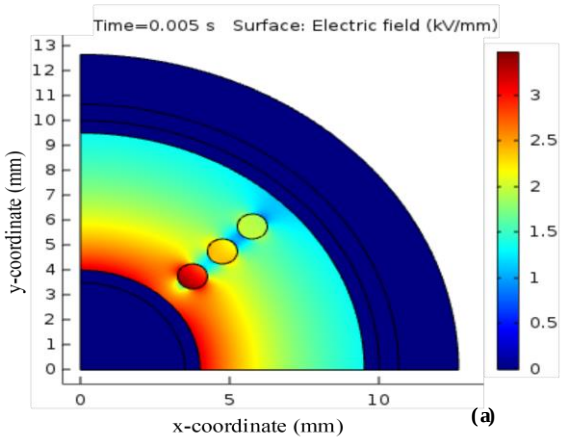

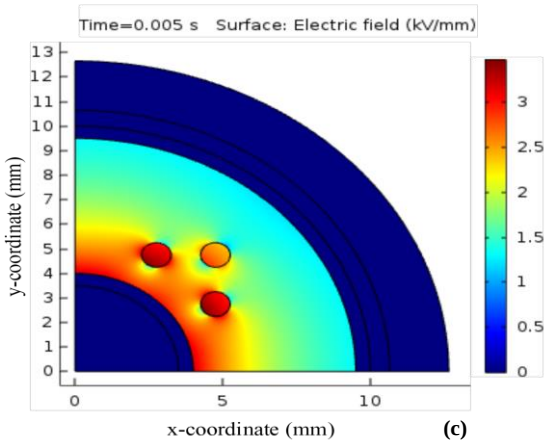

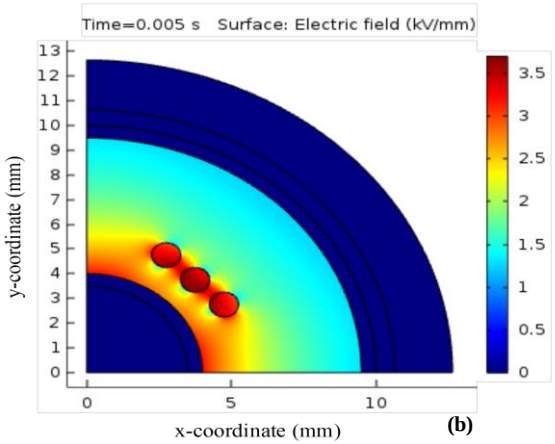

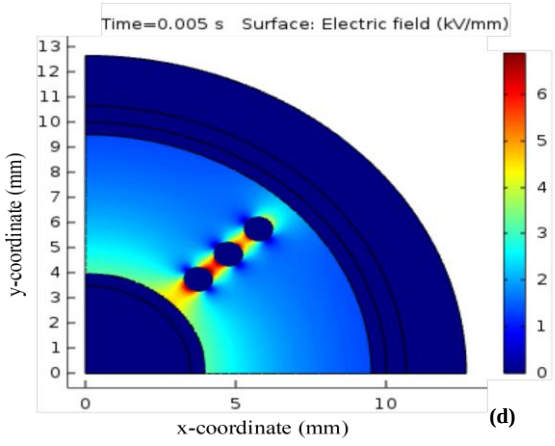

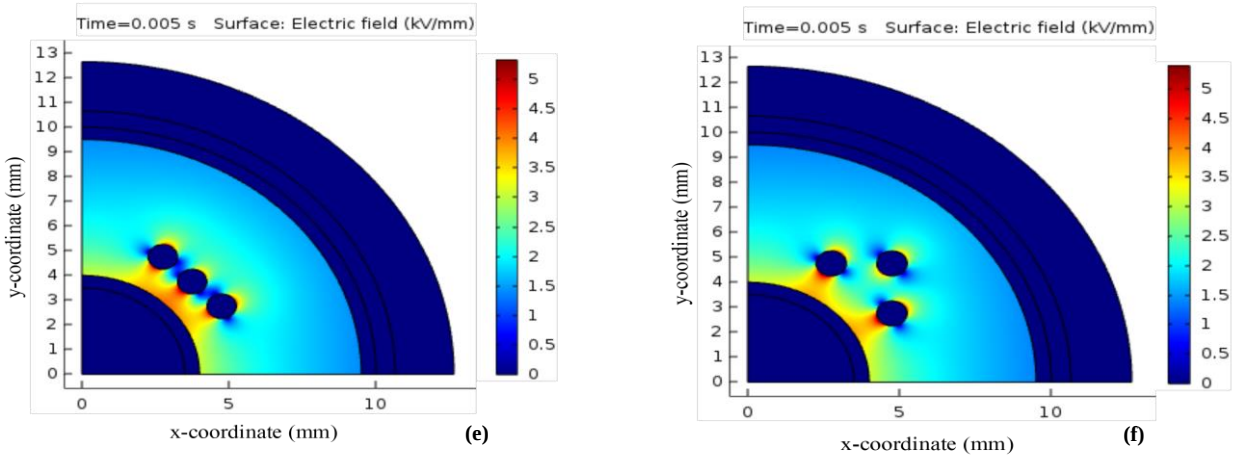

Figure 3. Electric field distribution with three cavities: prior to (a-c) and after initial PD (d-f)

is to be anticipated at the HV electrode. Field strength is stronger near the conductor's surface and decreases approaching the cable's ground potential. The average electric field strength is 3.0948 kV/mm, 2.3178 kV/mm, and 1.9400 kV/mm at the centre of cavities 1 (lower), 2 (middle), and 3 (upper) respectively. For cavities arranged horizontally (Figure 3b), there appears to be a slight change in the field intensity across the cavities.

In contrast to the vertical arrangement of cavities in Figure 3a, all cavities in this configuration are closer to the HV cable electrode. The middle cavity, 1, has a stronger electric field than the others (4 and 5), as well as the most insulation. This is practically due to the perpendicular nature of the source field to that cavity, i.e the middle cavity, 1. The middle cavity's average electric field magnitude is 3.5292 kV/mm, whereas the upper, 4, and lower, 5 cavities are 3.3247 and 3.3230 kV/mm, respectively. The results imply that for the horizontal arrangement of cavities, there is very little impact of a cavity on the other neighbouring cavities. This clearly shows higher interaction among the local field strength of horizontal cavities, thereby decreasing the level of the individual cavities' electric field strength.

Furthermore, for the triangular configuration of Figure 3c, the electric field intensity is greater in the first two cavities, 4, 5, than in the third cavity, 2 (i.e. the middle cavity). As expected, the two cavities (i.e. 4 and 5) closest to the conductor have a stronger electric field than the other. The average field values of the cavities are 2.5982 kV/mm, 2, 3.1982 kV/mm, 4, and 3.1974 kV/mm, respectively. The appearance of light-greenish colour, which produces zones of various electric field strengths throughout the insulation system, indicates the concentration of dynamic charges on the walls of the cavities. Generally, the field stack concentration is detected at the conductor-insulation contact and decreases towards the ground potential of the cable. Figures 3d, 3e, and 3f show the distribution of electric field strength magnitude after the first PD event. Charges deployed by the PD discharge on the cavity surface produce an electric field that opposes to the field established by the high voltage source and the electric field strength magnitude collapses and approaches zero.

For example, in Figure 3d, the average field strengths within the lower, 1, middle, 2, and upper, 3 cavities are 6.5142 $\times 10^{-7}$ kV/mm, 5.8632 $\times 10^{-7}$ kV/mm, and 4.7345 $\times 10^{-7}$ kV/mm, respectively. The field strength falls further from the conductor, reaching zero at the cable ground. For Figure 3e (i.e. horizontal arrangement of cavities), as expected there is a nearly consistent field distribution.

Figure 4 provides a magnified view of the electric field distributions of the model before and after a discharge event. Prior to the first PD, the change of field intensities, particularly in the cavities, is seen in Figs. 4a, 4b, and 4c. Similarly, in Figures 4d, 4e, and 4f, magnified views of field distributions following the first PD event are presented. While multiple colours (orange, grey, and light green) indicate the level of field intensities inside each cavity before the first PD, following PD, a single colour is achieved throughout all the cavities. This means that, regardless of the location of the cavity, the electric field strength after PD is always near to zero, as shown by the colour bar. Figure 5 depicts a graphical summary of the magnitudes of the electric fields in the three cavities before and after the first PD event.

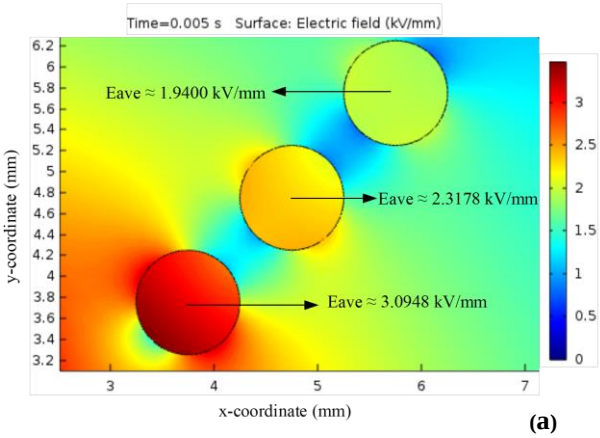

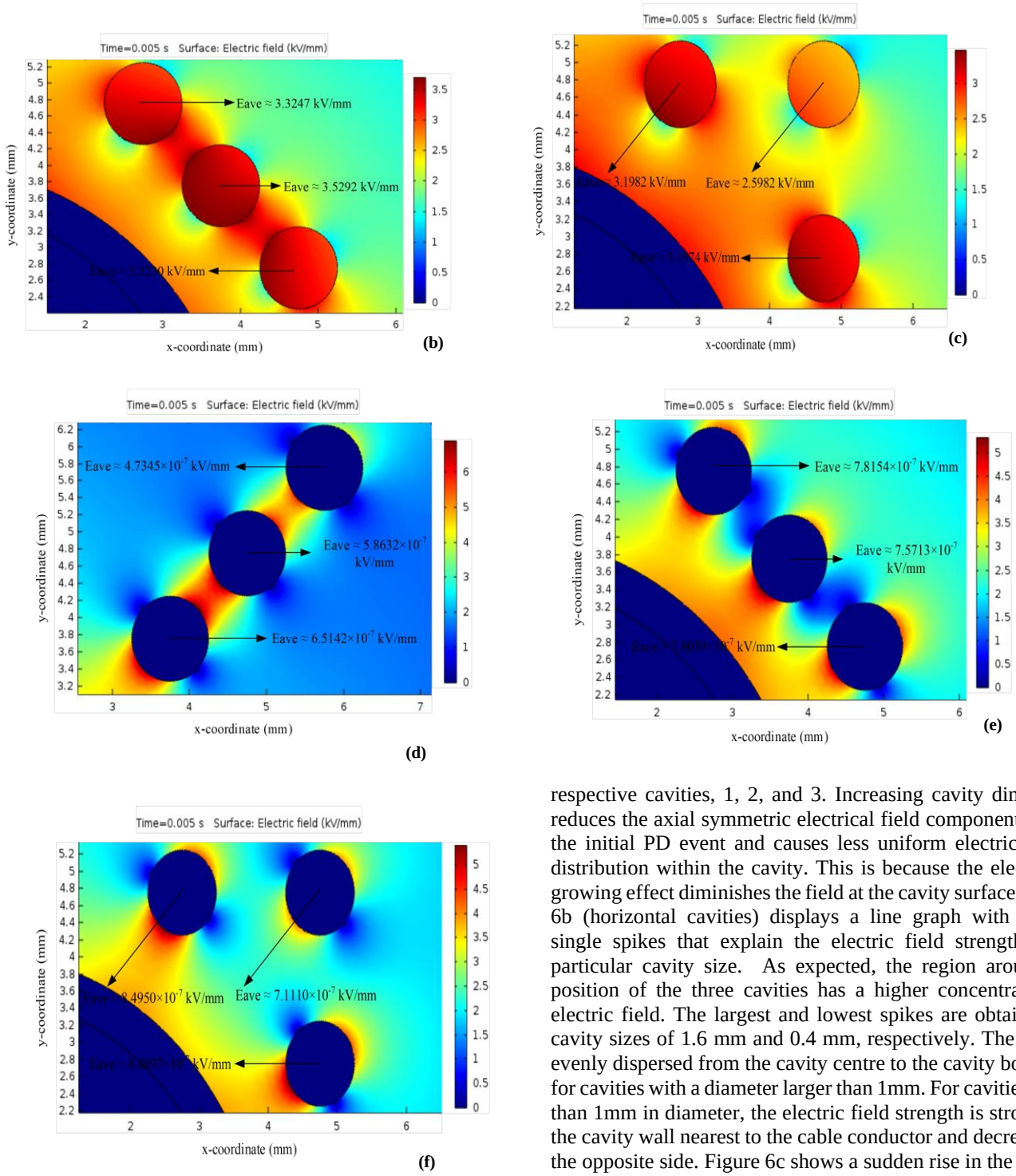

Figure 4. Magnified views of electric field distributions over the three cavities: prior to (left) and after initial PD (right)

Figure 6 depicts the distribution of electric fields along cut-line A. Figures 6a, 6b, and 6c show the electric field variation curves before the PD event for the vertical, horizontal, and triangular configurations. Fig. 6a shows the electric field variation at different points along cut-line A. Generally, the field graph shows several spikes of varying magnitude that correlate with the level of field intensities in the respective cavities, 1, 2, and 3. Increasing cavity dimension reduces the axial symmetric electrical field component before the initial PD event and causes less uniform electrical field distribution within the cavity. This is because the electrodes' growing effect diminishes the field at the cavity surface. Figure 6b (horizontal cavities) displays a line graph with several single spikes that explain the electric field strength for a particular cavity size. As expected, the region around the position of the three cavities has a higher concentration of electric field. The largest and lowest spikes are obtained for cavity sizes of 1.6 mm and 0.4 mm, respectively. The field is evenly dispersed from the cavity centre to the cavity boundary for cavities with a diameter larger than 1mm. For cavities lower than 1mm in diameter, the electric field strength is stronger at the cavity wall nearest to the cable conductor and decreases on the opposite side. Figure 6c shows a sudden rise in the electric field intensity caused by the cavity at the position 2.

Figures 6d, 6e, and 6f show the distributions of electric fields along cut-line A after the first PD event for vertical, horizontal, and triangular topologies, respectively. As expected, the field graphs in Figure 6d (vertically arranged cavities), generally show major reductions in the local field throughout each of the cavities. However, due to the increasing field intensity within the insulation system, the electric field rises again at the insulation cavity boundary. In Figure 6e (horizontally arranged cavities), as expected, there is also a decline in the field intensity around the three cavities.

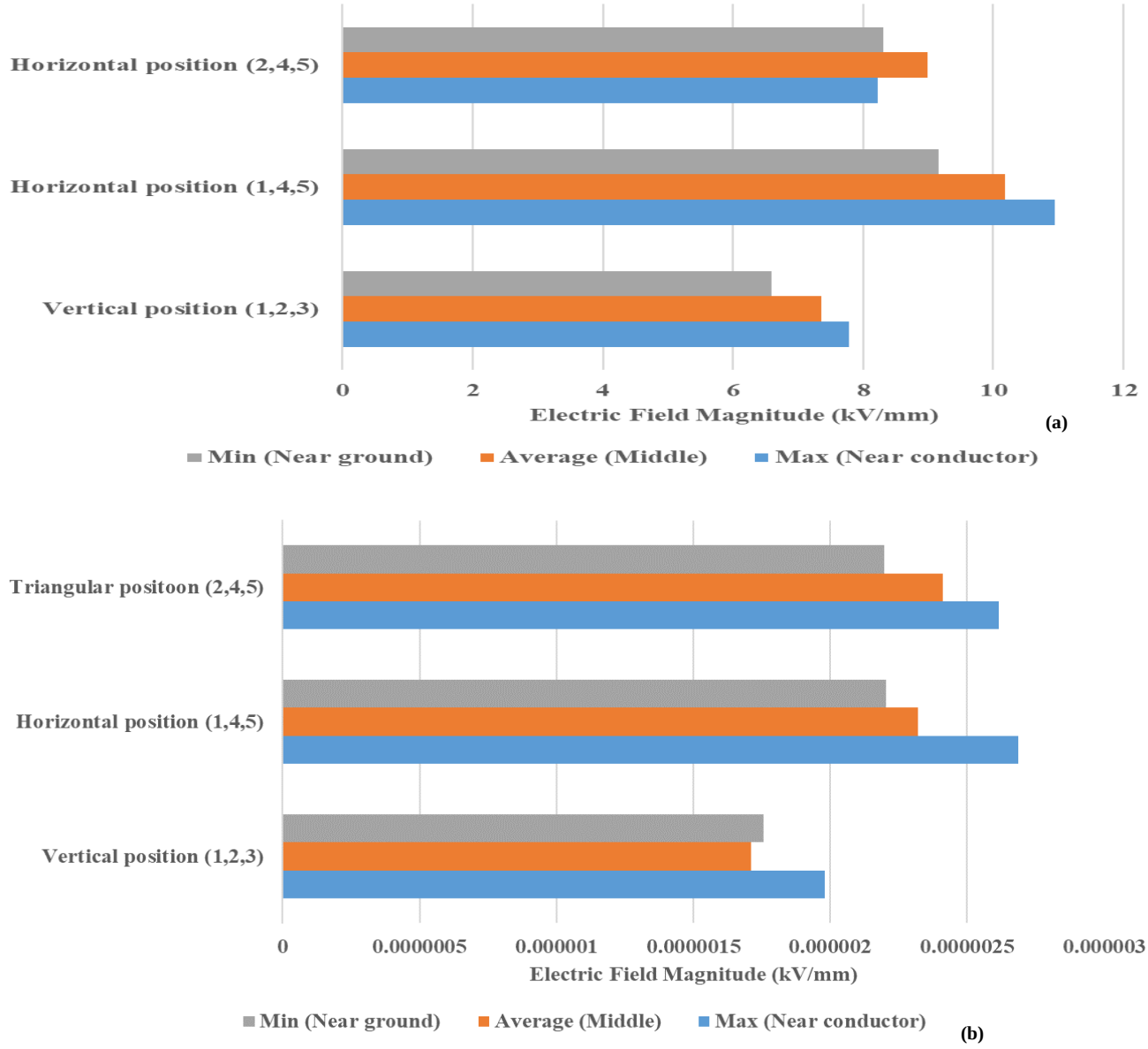

Figure 5. Comparison of electric field magnitudes within three cavities :(a) prior to PD and (b) after initial PD.

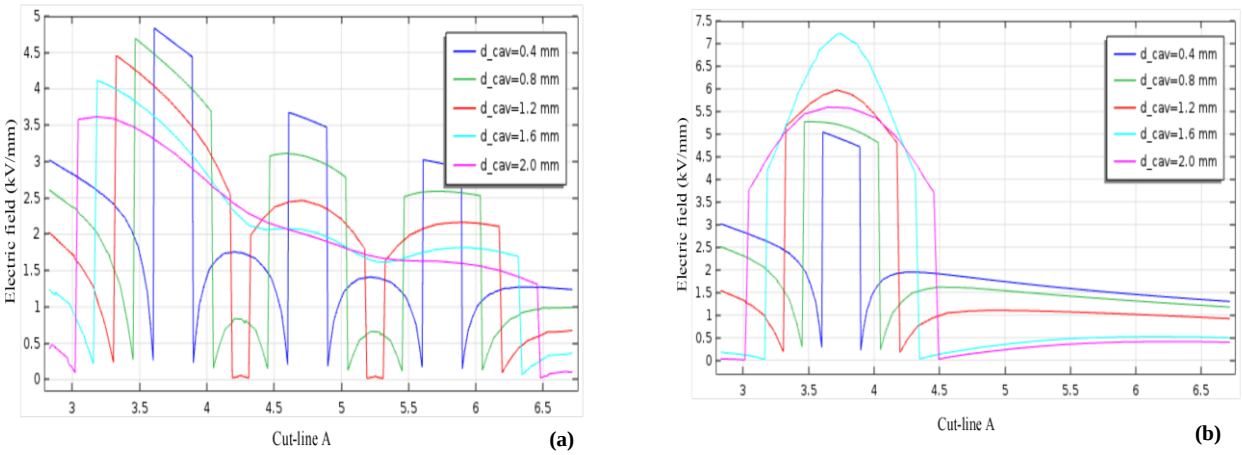

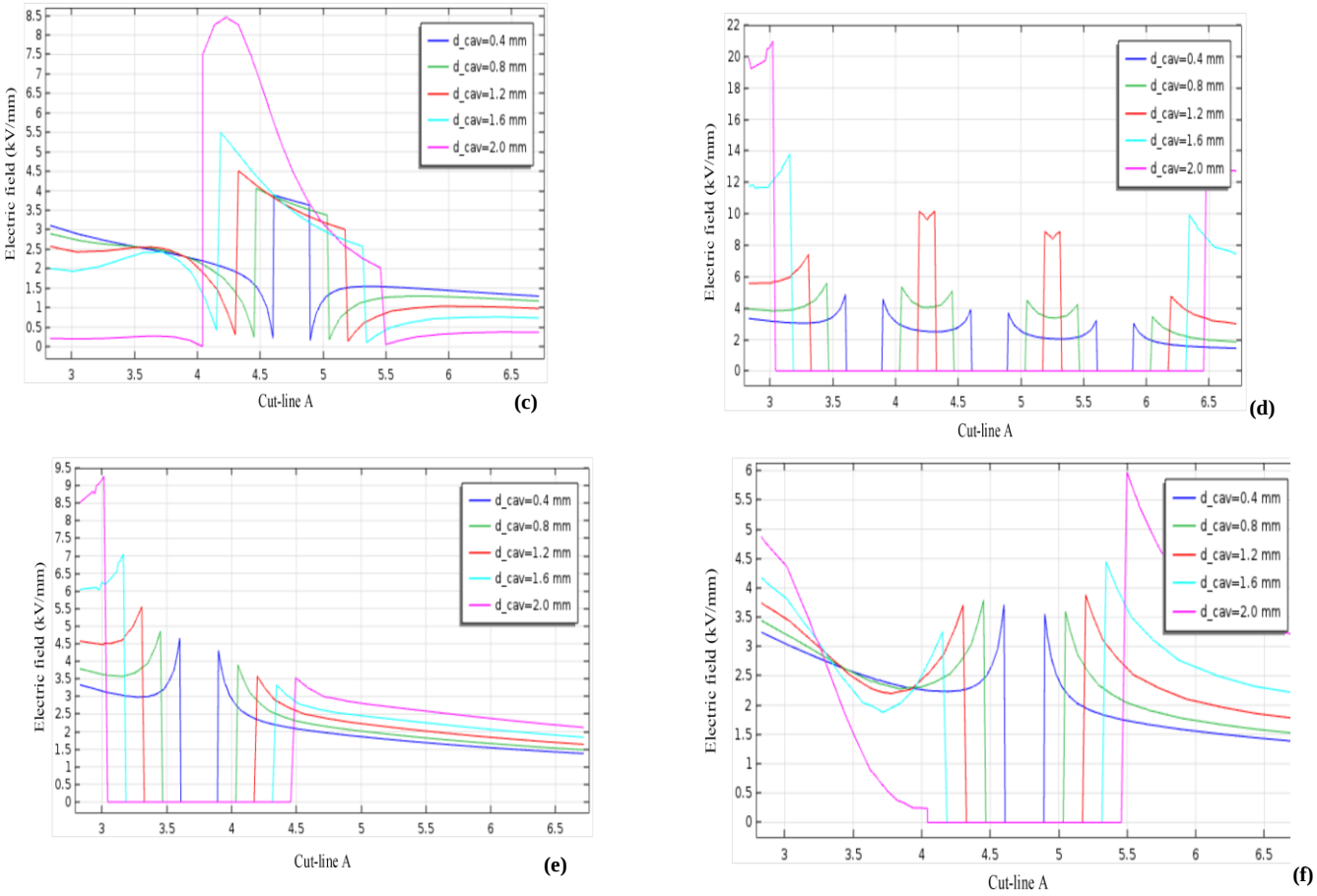

Figure 6. The distribution of electric field along cut-line A: prior to (a-c) and after initial PD (d-f) for different diameters of the cavities

Before that, the electric field is seen to vary depending on the cavity dimensions. Similarly, a huge drop in the electric field magnitude develops along the electric field graphs in Fig. 6f (triangular configurations). For a cavity diameter of 2.0 mm, the line graph follows a distinct pattern and appears to be lower at the cavity wall closest to the source field.

Figure 7 depicts the distributions of electric fields along cut-line B before and after the first PD event. Figures 7a-c show the field strength before the PD event while figures 7d-e show the field strength after the first PD event. In Fig. 7(a), the graph clearly shows the field strength across each cavity under consideration. For vertically arranged cavities, the cut-line B crosses over cavity, 1 only. Due to the close proximity of cavity 1 to the conductor, the electric field strength is higher at the cavity position than the other part of the insulation. Generally, the magnitudes of the graphs change with variations in as a function of the cavities. There is also a slight drop in the field at the cavity 1 position, and rises with an increase in cavity dimensions. This is because of the electric field interaction between the cavity and the conductor thereby reducing the intensity of the electric field at that location. For horizontally arranged cavities (Figure 7b), the electric field strength magnitude distribution exhibits a completely different pattern, when compared with vertically arranged cavities. Due to high electric field intensity at the middle cavity, 1, a dip is seen in the centre of the field graphs for cavity sizes of 0.4 mm and 0.8 mm. Additionally, for arbitrary configurations (Fig. 7c), two spikes of identical magnitude are seen at the upper part of the graphs. This is due to the electric field intensities at cavities 4 and 5 respectively.

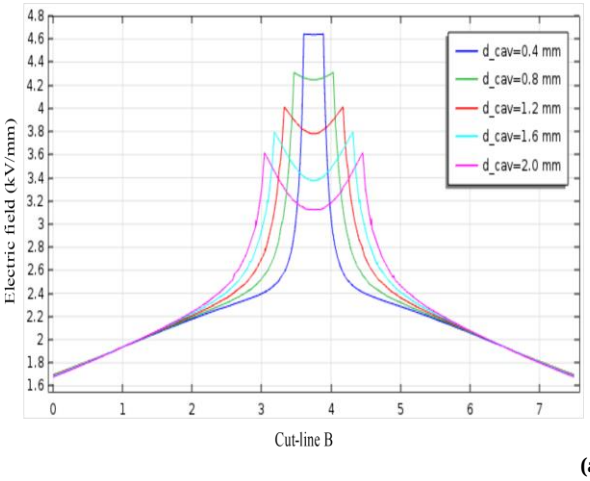

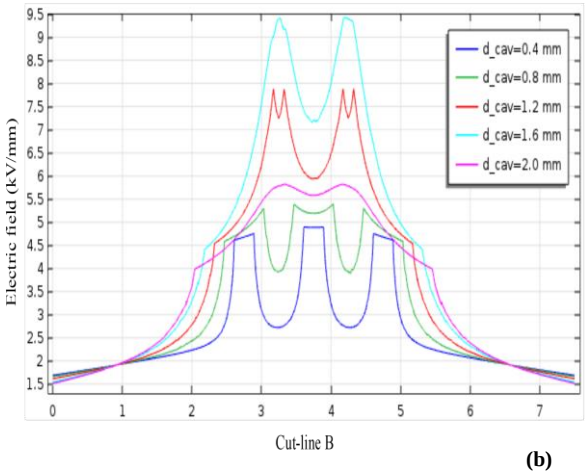

(b)

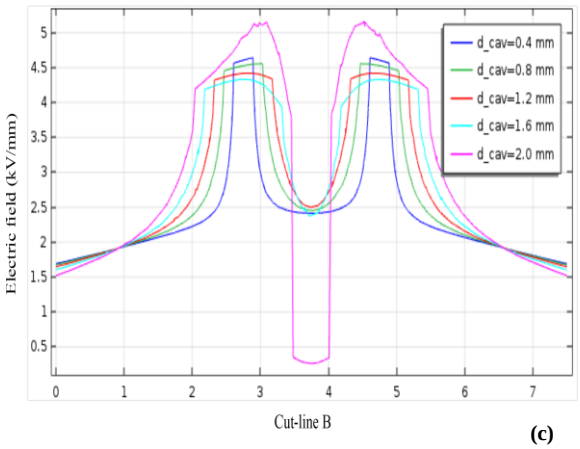

(c)

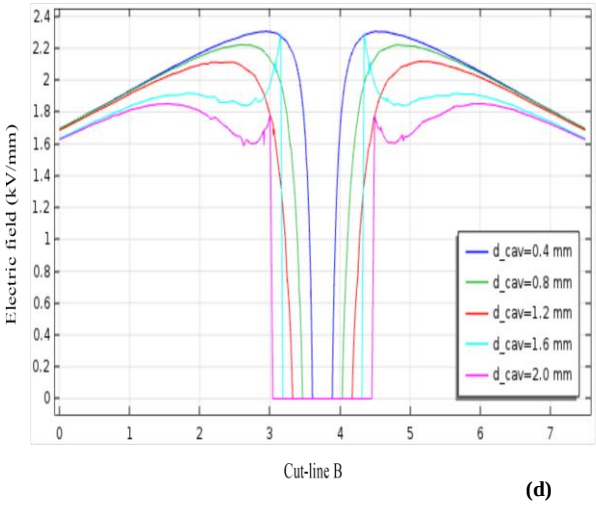

(d)

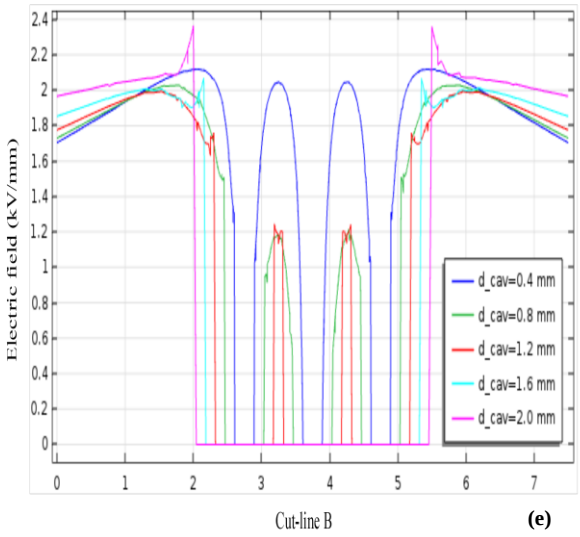

(e)

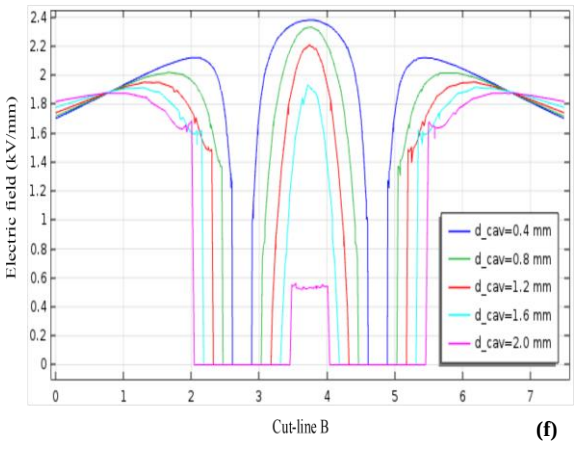

(f)

Figure7. The distribution of Electric field along cut-line B: prior to (a-c) and after initial PD (d-f) for different diameters of the cavities.

Figures 7(d), 7(e), and 7(f) show the field distribution along cut-line B, after the initial PD activity. For vertically arranged cavities in Fig. 7(d), a reduction in the electric field amplitude has been observed in the cavity, 1. In Figure 7(e), i.e. horizontally arranged cavities, three large dips at the middle of the plots reflect the low field intensity throughout the three cavities, 1, 4, and 5. The two dips at the middle of the plots (i.e. arbitrarily configurations) in Fig. 7(f), show a dip in the electric field strength across the cavities 4 and 5.

B. Evaluation and comparison of average electric field strengths

Figure 8 compares the mean electric field magnitudes measured at three positions across the cable insulation with and without the three cavities. The highest (10.1769 kV/mm) and lowest (7.3526 kV/mm) average fields across the defected cable model has been recorded for the horizontal and triangular configurations. Identical results can also be seen for the healthy cable, although as expected lower electric field values are recorded. The percentage increment in the electric field strength for the vertical, horizontal and triangular configurations with or without the three cavities is 20.4%, 30.9% and 27.4% respectively. Among them, the horizontal configuration has the greatest value due to higher interaction and superposition of the electric field produced by the cavities.

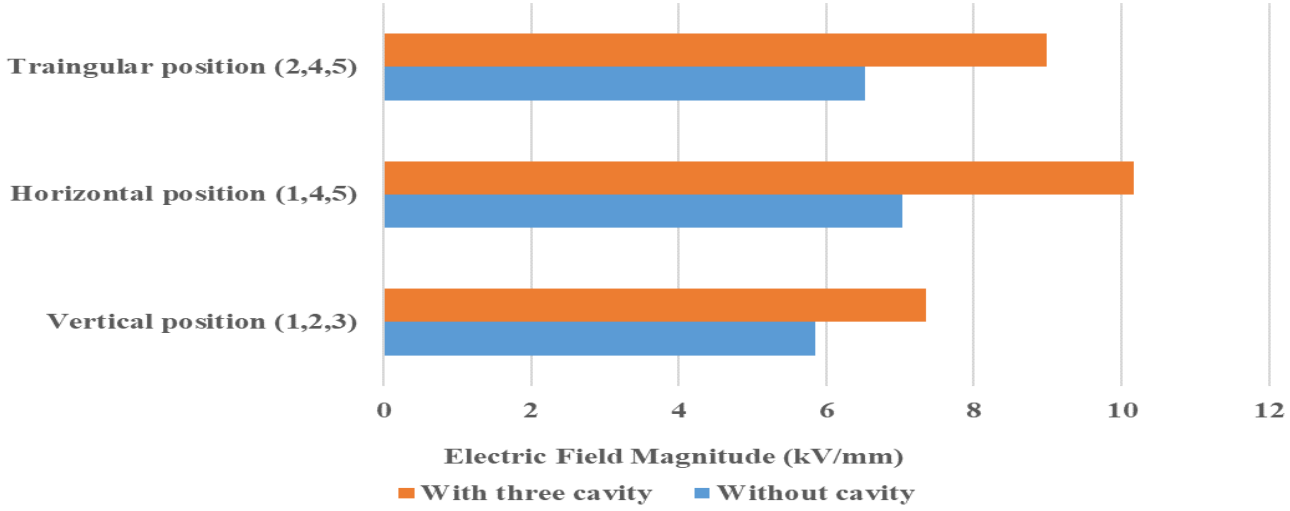

Figure 8. Comparison of average electric field magnitudes without and with three cavities in parallel, series and triangular configurations

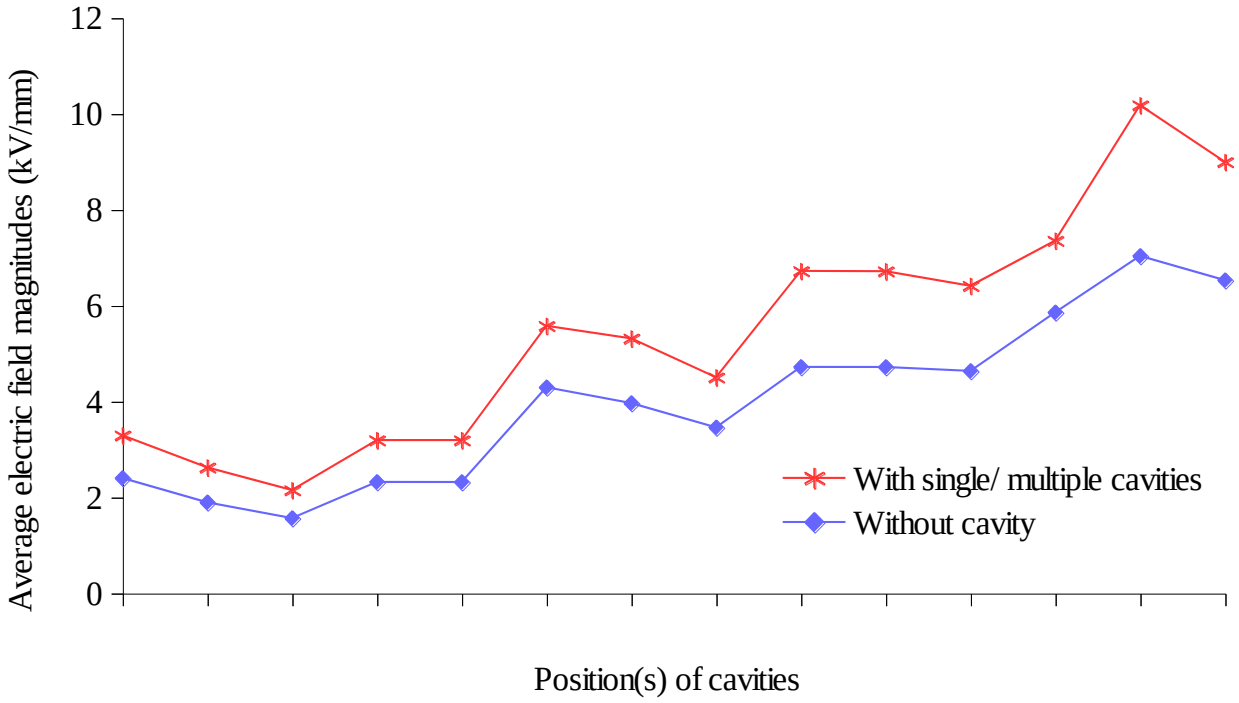

Figure 9. Comparison of percentage average field contributions in two and three cavities arranged vertically, horizontally and in a triangular shape.

Figure 9 shows a single-line plot of the percentage field contributions due to single and multiple cavities at different positions and configurations. The percentage increase in the average field strength due to the presence of multiple cavities of various configurations is compared to the total average of original fields (2.0978 kV/mm), and the results shown in Figure 9. When compared with the original case, without cavities, it was found that the field strength magnitude increases by 62.7% for the vertical configuration, 68.7% for horizontal configuration and 67.3% for triangular configuration.

V. CONCLUSION

In this study, the field distributions and the behaviour of PD in XLPE insulated power cables under different test and cavity dimensions have been investigated. Specifically, three cavity configurations have been considered i.e. vertical, horizontal and triangular. COMSOL Multiphysics software has been utilized to create a two-dimensional model of a three-core XLPE insulated power cable. During the simulation process, two cases were considered i.e., a healthy cable (without PD) and an unhealthy cable (with PD). The major results can be summarised as follows:

- For the vertical arrangement of cavities, the higher the distance of the cavity from the conductor, the lower its electric field strength. This is true for both healthy and unhealthy cables, although the electric field is nearly zero after the occurrence of the PD. This is because the PD activity generates an opposing electric field that reduces electric field strength on the cavity surface.
- For the horizontal arrangement of cavities, there is very little impact of a cavity on the neighbouring ones. This clearly shows higher interaction among the local field strength of horizontal cavities, thereby decreasing the level of the individual cavities electric field strength.
- The percentage increment in the field strength for the vertical, horizontal and triangular configurations with or without the three cavities is 20.4%, 30.9% and 27.4% respectively. Among them, the horizontal configuration has the greatest value due to higher interaction and superposition of the electric field produced by the cavities.
- Finally, the percentage field increase for vertical, horizontal, and triangular topologies is 62.7%, 68.7%, and 67.3%, respectively, when compared to the initial electric field without cavities.

AUTHOR CONTRIBUTIONS

The authors have contributed in different parts of the paper preparation, as follows, Conceptualization, methodology and analysis, **U. Musa and A.A. Mas'ud;** software and simulations, **U. Musa.**; writing— original draft preparation, **U. Musa;** writing—review and editing, **A.A. Mati, G.S. Shehu, S.H. Sulaiman and J.M. Rodriguez-Serna.**

REFERENCES

Afia, R.S.; E. Mustafa and Z.Á. Tamus. (2021). Comparison of Mechanical and Low-Frequency Dielectric Properties of Thermally and Thermo-Mechanically Aged Low Voltage CSPE/XLPE Nuclear Power Plant Cables. Electronics, 10(22):2728: 1-15.

Alsharif, M.; P.A. Wallace; D.M. Hepburn and C. Zhou. (2012). FEM modelling of electric field and potential distributions of MV XLPE cables containing void defect. In Excerpt from the Proceedings of the 2012 COMSOL Conference, Milan, Italy, 1-4.

Choudhary, M.; M. Shafiq; I. Kiitam; A. Hussain; I. Palu and P. Taklaja. (2022). A Review of Aging Models for Electrical Insulation in Power Cables. Energies, 15(9):3408: 1-20.

do Nascimento, D.A.; S.S. Refaat; A. Darwish; Q. Khan; H. Abu-Rub and Y. Iano. (2019). Investigation of void size and location on partial discharge activity in high voltage XLPE cable insulation. Paper presented at the 2019 Workshop on Communication Networks and Power Systems (WCNPS), Brasilia, Brazil,1-6. IEEE.

Feng, X.; Q. Xiong; A.L. Gattozzi and R.E. Hebner. (2020). Partial discharge experimental study for medium voltage DC cables. IEEE Transactions on Power Delivery, 36(2): 1128-1136.

Gouda, O.E.; A.A. ElFarskoury; A.R. Elsinnary and A.A. Farag. (2018). Investigating the effect of cavity size within medium-voltage power cable on partial discharge behaviour. IET Generation, Transmission & Distribution, 12(5): 1190-1197.

Gutfleisch, F. and Niemeyer, L. (1995). Measurement and simulation of PD in epoxy voids. IEEE transactions on Dielectrics and Electrical insulation, 2(5): 729-743.

Joseph, J.; S. Mohan and S. Thiruthi Krishnan. (2019). Numerical modelling, simulation and experimental validation of partial discharge in cross-linked polyethylene cables. IET Science, Measurement & Technology, 13(2): 309-317.

Kuffel, J. and Kuffel, P. (2000). High voltage engineering fundamentals. Pergamon Press, 1984.

Mas' ud, A.A.; J.A. Ardila-Rey; R. Albarracín and F. Muhammad-Sukki. (2017). An ensemble-boosting algorithm for classifying partial discharge defects in electrical assets. Machines, 5(3):18 :2-13.

Mas'ud, A.A.; B.G. Stewart and S.G. McMeekin. (2016). An investigative study into the sensitivity of different partial discharge φ-qn pattern resolution sizes on statistical neural network pattern classification. Measurement, 92: 497-507.

Meziani, M.; A. Mekhaldi and.M. Teguar. (2016). Effect of space charge layers on the electric field enhancement at the physical interfaces in power cable insulation. IEEE Transactions on Dielectrics and Electrical Insulation, 23(6): 3725-3733.

Morsalin, S. and Phung, T. (2020). Electrical field distribution on the cross-linked polyethylene insulation surface under partial discharge testing. Polymer Testing, 82: 106311.

Morsalin, S.; B.T. Phung and A. Cavallini. (2020). Measurement and modeling of partial discharge arising from different cavity geometries at very low frequency. IEEE Transactions on Dielectrics and Electrical Insulation, 27(4): 1110-1118.

Morshuis, P.H. (2005). Degradation of solid dielectrics due to internal partial discharge: some thoughts on progress made and where to go now. IEEE Transactions on Dielectrics and Electrical Insulation, 12(5): 905-913.

Musa, U.; A.A. Mati; A.A. Mas' ud; G.S. Shehu; R. Albarracin-Sanchez and J.M. Rodriguez-Serna. (2021). Modeling and analysis of electric field variation across insulation system of a MV power cable. Paper presented at the International Conference on Electrical, Communication, and Computer Engineering (ICECCE), Kuala Lumpur, Malaysia: 1-5, USA: IEEE.

Pan, C.; G. Chen; J. Tang and K. Wu. (2019). Numerical modeling of partial discharges in a solid dielectric-bounded cavity: A review. IEEE Transactions on Dielectrics and Electrical Insulation, 26(3): 981-1000.

Pandey, J.C. and Singh, M. (2021). Dielectric polymer nanocomposites: Past advances and future prospects in electrical insulation perspective. SPE Polymers, 2(4): 236-256.

Ragusa, A., Sasse, H. and Duffy, A.P. (2020). 3D Model of partial discharge in defects with different sizes and positions in power cable for distribution and transmission networks. IET Science, Measurement & Technology, 14(9): 776-783.

Refaat, S.S. and Shams, M.A. (2018). A review of partial discharge detection, diagnosis techniques in high voltage power cables. Paper presented at the 12th International

Conference on Compatibility, Power Electronics and Power Engineering (CPE-POWERENG 2018), Doha, Qatar, 1-5. IEEE.

Rodríguez-Serna, J.M. and Albarracín-Sánchez, R., (2019). Numerical simulation of temperature and pressure changes due to partial discharges in spherical cavities within solid dielectrics at different ageing conditions. Energies, 12(24):4771: 1-11.

Rodríguez-Serna, J.M.; R. Albarracín-Sánchez and A.A. Mas' ud, (2020). Finite-element-analysis models for numerical simulation of partial discharges in spherical cavities within solid dielectrics: a review and a novel method. High Voltage, 5(5), pp.556-568.

Sharshir, A.I.; S.A. Fayek; A. El-Gawad; M.A. Farahat; M.I. Ismail and M.M. Ghobashy. (2022). Experimental investigation of E-beam effect on the electric field distribution in cross- linked polyethylene/ZnO nanocomposites for medium-voltage cables simulated by COMSOL Multiphysics. Journal of Analytical Science and Technology, 13(1): 1-13.

Subramaniam, A.; A. Sahoo; S.S. Manohar; S.J. Raman and S.K. Panda. (2021). Switchgear Condition Assessment and Lifecycle Management: Standards, Failure Statistics, Condition Assessment, Partial Discharge Analysis, Maintenance Approaches, and Future Trends. IEEE Electrical Insulation Magazine, 37(3): 27-41.

Zhang, X.; B. Pang; Y. Liu; S. Liu; P. Xu; Y. Li; Y. Liu; L. Qi and Q. Xie. (2021). Review on detection and analysis of partial discharge along power cables. Energies, 14(22): 7692.